

Magnetic Properties of Fe and Ni Doped SnO₂ Nanoparticles

Regular paper

Aditya Sharma^{1*}, Mayora Varshney¹, Shalendra Kumar², K.D.Verma¹ and Ravi Kumar³

1 Material Science Research Laboratory, Department of Physics, S.V.College, India

2 School of Nano & Advance Materials Engineering, Changwon National University, Republic of Korea

3 Centre for Materials Science and Engineering, National Institute of Technology, India

*Corresponding author E-mail: adityaiuac@gmail.com

Received 8 May, 2011; Accepted 30 June, 2011

Abstract In this work, we report the room temperature ferromagnetism in Sn_{1-x}Fe_xO₂ and Sn_{1-x}Ni_xO₂ (x = 0.00, 0.03 and 0.05) nano-crystalline powders. All the samples were prepared using co-precipitation method. X-Ray Diffraction (XRD), transmission electron microscopy (TEM), energy dispersive x-ray analysis (EDAX), UV-visible absorption spectroscopy and room temperature magnetization measurements were performed to study the crystal structure, morphology, elemental analysis, optical band gap and magnetic properties of Fe and Ni doped SnO₂. TEM results depict the formation of spherically shaped and small sized nanoparticles of the diameter of ~ 3 nm. The band gap energy of the Fe and Ni doped samples found to decrease with increasing their concentrations. The higher saturation magnetization was observed in low concentration Fe and Ni doped tin oxide.

Key Words Nanoparticles, XRD, DMS, ferromagnetism.

1. Introduction

Among the various important categories of the functional materials like; polymers, magnetic, dielectric and semiconductors, the ferromagnetic semiconductors are emerged as attracting materials and driven a considerable attention in the recent years [1-2]. To have a magnetic

semiconductor, a non-magnetic semiconductor is doped with transition metal ions to achieve magnetism from it. It is further found that the transition metal impurity is of only few percent of the cations, i.e., it is very dilute. Due to this reason such material are known as *Diluted Magnetic Semiconductor (DMS)*. Such materials promise to provide a wide range of applications in various fields like logic, storage, communications, quantum computation and multi-functionality on the same chip [3]. For realizing this goal it is very necessary that the magnetism in these DMS systems should be carrier-mediated. It is known that the number of charge carriers in a semiconductor can be tuned with the application of electric voltages, so if the magnetism is charge carriers mediated then this will give a handle to control the magnetism in the system with the help of applied electrical signals and will increase the multi-functionality of the material. The study of DMS materials is being carried out since last few decades. Apart from the present day applications in the field of Spintronics, they are interesting to the physics community due to the rich variety of phenomena and physics they exhibit [4]. Preparation of single phase DMS, devoid of any secondary phases or metallic clusters, is a big challenge. More often it turns out that the system is having impurity phases when the system is characterized using various complimentary techniques. Even if the

material is single phases, the reports on the same system, prepared under same conditions by various groups are very contradictory. Apart from the issue of reproducibility, the magnetism in these systems has always been controversial and the debate on the origin and the mechanism of ferromagnetism is far from over. One of the most widely studied system and the one in which carrier-mediated ferromagnetism has been established is the (Ga,Mn)As system. But the problem is its low Curie temperature ($T_c = 150$ K) [5]. To use these materials in industry for the device applications, their Curie temperature should be well above room temperature (> 400 K). One of the most important predictions on preparation of DMS showing above room temperature ferromagnetism (RTFM) was made based on the mean-field theoretical treatments using the Zener exchange mechanism [6]. According to their calculations 5 % Mn doped ZnO and GaN were expected to show RTFM for a hole concentration of $3.5 \times 10^{20} \text{ cm}^{-3}$. The holes in the valence band have a strong exchange interaction with the magnetic impurity. Due to this reason these holes can mediate an indirect exchange coupling among the doped transition metal ions, which lead to the long range ordering and to RTFM, as well as spin-splitting of the electronic states proportional to the magnetization of the doped ions. Following these predictions there were flurry of reports from all over the globe on the transition metal doped ZnO and other oxide semiconductor materials. The main difficulty in preparing *p*-type oxides semiconductor materials [7] is the large *n*-type background that is most of the time present in the oxide systems. This brings to another problem in the oxides. This *n*-type background is conventionally attributed to the defects like O vacancies and metal interstitials. Therefore, it is difficult to establish a mechanism to explain origin of room temperature ferromagnetism in the oxide systems.

Among the other known oxide semiconductors, tin oxide (SnO_2) is a very interesting oxide material with a wide band gap of 3.6 eV. Its higher optical transparency, chemical stability, and electrical conductivity make it a very attractive material for solar cells, catalysis and gas sensing applications. In the nano-scale form TM-doped SnO_2 is reported to demonstrate more interesting structural and magnetic properties. For instance, chemically synthesized Co-doped SnO_2 exhibit different size/shape features with increasing Co content. Moreover, very low magnetic moments ($0.133 \mu_B/\text{Co}$) with a high coercivity (~ 630 Oe) were also observed [8]. In the thin film form, Co doped SnO_2 shows high magnetic moment ($\sim 7.5 \mu_B/\text{Co}$) with low coercivity (~ 50 Oe) [9]. In the Mn-doped SnO_2 system, the magnetic moments per Mn site were found to decrease with increasing Mn content, x , indicating an anti-ferromagnetic (AFM) nature of Mn-O-Mn interaction, reminiscent of AFM in rutile MnO_2 [10]. It

was also suggested that the exchange interaction mechanism of the observed RTFM in $\text{Sn}_{1-x}\text{M}_x\text{O}_2$ ($M = \text{Mn}$ & Fe) powders involve an electron trapped at an oxygen vacancy adjacent to the transition metal ion (F-centre exchange) [11]. Till date the origin of ferromagnetism still remains indistinct in so far proposed DMS systems because of their multi phase nature etc. In this study we report the room temperature ferromagnetism in chemically synthesized, single phase, Fe and Ni doped tin oxide nanoparticles.

2. Experimental Details

All the reagents used were of analytical grade without further purification. 0.01M solutions of $\text{SnCl}_4 \cdot 5\text{H}_2\text{O}$, $\text{NiCl}_2 \cdot 5\text{H}_2\text{O}$ and $\text{FeCl}_2 \cdot 5\text{H}_2\text{O}$ were prepared with a molar ratio of $x = \text{Fe}/(\text{Fe}+\text{Sn})$ and $\text{Ni}/(\text{Ni}+\text{Sn})$ by proper dissolving into de-ionized water. Ammonium Hydroxide (NH_4OH) was added into the solution (drop by drop), with stirring, until the white precipitates were obtained. After 30 minutes of stirring the resultant mixtures were rinsed, several times, with de-ionized water to remove chlorine and other ionic impurities, which may formed during the synthesis process. These washed precipitates were dried in air at 40°C for 20 hours followed by natural cooling up to the room temperature and then final powder products were collected carefully. A detailed characterization of the samples was carried out using XRD, TEM, EDAX, UV-visible spectroscopy and dc-magnetization measurements. XRD patterns were obtained using Bruker D8 advanced diffractometer using $\text{CuK}\alpha$ radiation ($\lambda = 1.540 \text{ \AA}$) operated at voltage 40 kV and current of 40 mA. TEM measurements were performed using FEI-Tecnai-20 transmission electron microscope operated at 200 kV. Optical absorption spectra were recorded with the conventional two beam method using Hitachi UV-3300, UV-VIS spectrometer. Room temperature magnetization measurements were performed using commercial quantum Design physical properties measurement system (PPMS).

3. Results and Discussion

Fig. 1 (a) – (e) show the XRD patterns of $\text{Sn}_{1-x}\text{Fe}_x\text{O}_2$ ($x = 0.0, 0.03, \text{ and } 0.05$) $\text{Sn}_{1-x}\text{Ni}_x\text{O}_2$ ($x = 0.03 \text{ and } 0.05$) nanoparticles, respectively. It is clearly evident from Fig.1 that the peaks corresponding to the rutile-type SnO_2 are detected for all compositions, indicating Fe and Ni doping does not affect the original tetragonal unit cell of SnO_2 . However, the observed XRD peaks are quite wider and having sufficient background. This kind of broad XRD peaks, with high background, have also been reported in case of very small sized SnO_2 quantum dot/nanoparticles [12-13]. The peak broadening and high background may arise due to the (i) poor performance of used diffractometer and (ii) very narrow size distribution of the so formed

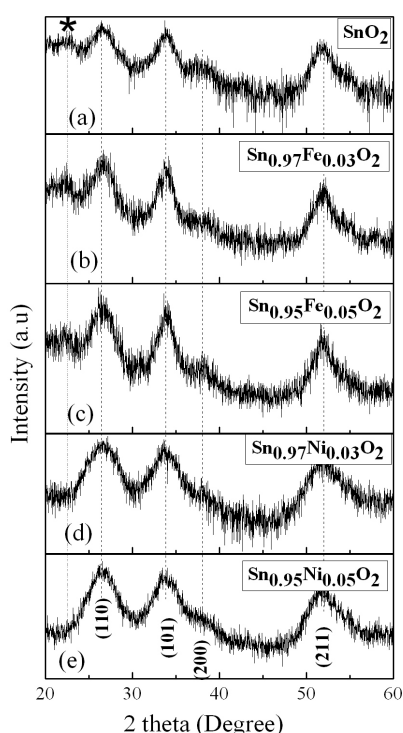


Figure 1. (Color online) XRD patterns of (a) SnO_2 , $\text{Sn}_{0.97}\text{Fe}_{0.03}\text{O}_2$ and $\text{Sn}_{0.95}\text{Fe}_{0.05}\text{O}_2$ (b) $\text{Sn}_{0.97}\text{Ni}_{0.03}\text{O}_2$ and $\text{Sn}_{0.95}\text{Ni}_{0.05}\text{O}_2$ nanoparticles, respectively.

nanoparticles/quantum dots. In the present case, the small size of the as-synthesized nanoparticles may be responsible for the XRD peak broadening. Moreover, an extra peak is present in un-doped and doped samples (marked by asterisk). This peak, appearing at $\sim 22^\circ$, does not match with any phase of SnO , Sn_2O_3 , Sn_3O_4 or even phases of Fe_2O_3 and Fe_3O_4 , as verified from the corresponding JCPDS files. This peak may belong to some organic phase formed during the growth of nanoparticles by the chemical method. Similar kind of organic phases have also been reported in the TiO_2 thin films, deposited by chemical coating method [14]. The average grain sizes were calculated from XRD patterns using the Scherrer

relation; ($D=0.9\lambda/\beta\cos\theta$, where β is FWHM of the XRD peaks and λ is the wavelength of incident x-rays). Thus calculated average grain size falls in the small size regime of ~ 3.5 nm in all the samples, prepared with different concentrations of Fe and Ni.

To further confirm the particle size, morphology and elemental concentration of as-prepared samples, systematic TEM and EDAX measurements were performed. Fig. 2 (a - c) shows the TEM images of (a) SnO_2 , (b) $\text{Sn}_{0.95}\text{Fe}_{0.05}\text{O}_2$ and (c) $\text{Sn}_{0.95}\text{Ni}_{0.05}\text{O}_2$ samples, respectively. It is clear from the figure that spherical shaped nanoparticles have been formed in un-doped and TM ion doped SnO_2 . However, some aggregation of nanoparticles has been observed in all TEM micrographs. This aggregation in wet chemically synthesized nanoparticles is expected due to the presence of substantial OH^- ions in samples [15]. This aggregation makes it difficult to determine crystal size accurately. The average size, which is estimated from individual spherical nanocrystals, is ~ 3.1 nm, 3.6 nm and 3.4 nm for SnO_2 , $\text{Sn}_{0.95}\text{Fe}_{0.05}\text{O}_2$ and $\text{Sn}_{0.95}\text{Ni}_{0.05}\text{O}_2$ samples, respectively. Thus calculated particle sizes are in very good agreement to those calculated from XRD data. Fig. 3 (a-e) shows the EDAX spectra, collected from the average scanned area, of un-doped SnO_2 , $\text{Sn}_{0.97}\text{Fe}_{0.03}\text{O}_2$, $\text{Sn}_{0.95}\text{Fe}_{0.05}\text{O}_2$, $\text{Sn}_{0.97}\text{Ni}_{0.03}\text{O}_2$ and $\text{Sn}_{0.95}\text{Ni}_{0.05}\text{O}_2$ samples, respectively. The self-generated elemental composition (wt. %) details are also presented in Fig. 3. It is clear from Fig. 3 that Sn, and O are only the main elemental species in pure SnO_2 sample while, additionally, Fe and Ni peaks were observed in Fe and Ni doped samples. However, C peaks, very close to the O peaks, were also observed in all the samples. These C peaks were eliminated from the EDAX spectra, during the data analysis, to better examine the O peaks in the spectra. Moreover, the weight percentage of the doped transition metal elements was found to be little higher than that of nominal concentration, used during the calculations and sample preparation.

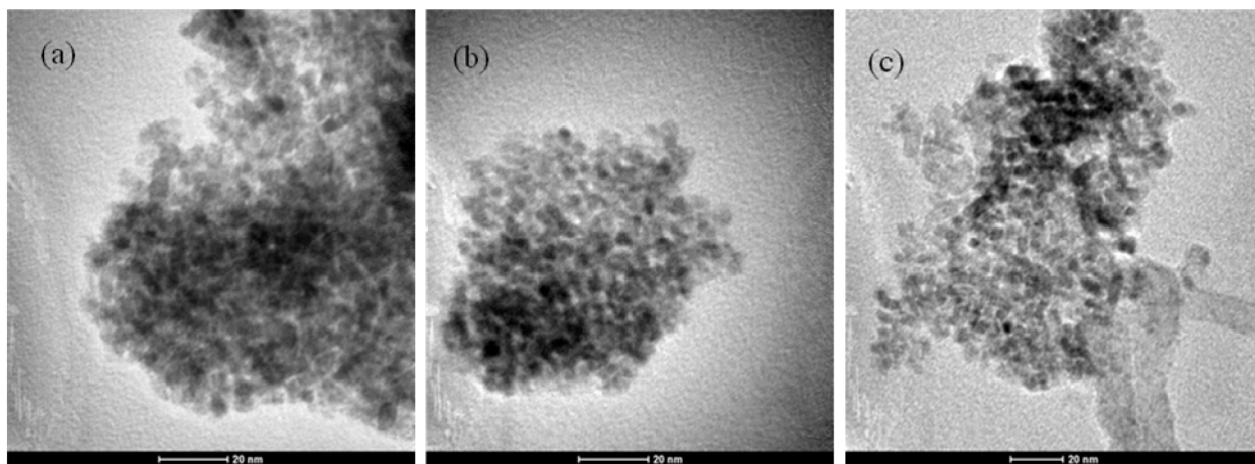


Figure 2. TEM images of (a) SnO_2 , (b) $\text{Sn}_{0.95}\text{Fe}_{0.05}\text{O}_2$ and (c) $\text{Sn}_{0.95}\text{Ni}_{0.05}\text{O}_2$ nanoparticles, respectively.

To study the optical properties and the effect of Fe and Ni doping on the optical band gap of SnO₂ nanoparticles, systematic, UV-visible absorption spectra were recorded in the incident photon wavelength of 200 nm to 600 nm. The Fig. 4 shows the absorption spectra of SnO₂, Sn_{0.95}Fe_{0.05}O₂, and Sn_{0.95}Ni_{0.05}O₂ nanoparticles, respectively. The inset of the figure shows the Tauc's plot for determining the band gap energy of nanoparticles. The estimated band gap energy of un-doped SnO₂ is ~4.1 eV, while, the band gap energy of the Fe and Ni doped compounds (for x = 0.05) found to almost same and is ~3.87 eV. The observed band gap energy of un-doped SnO₂ nanoparticles is quite higher than the band gap energy of bulk SnO₂ (3.6 eV). The appearance of such larger band gap energy is expected in SnO₂ nanoparticles because of their small size of ~3 nm. This observation is consistent with the previously reported large band gap energy in SnO₂ nanoparticles and nano-rods [15]. Sn_{1-x}Fe_xO₂ and Sn_{1-x}Ni_xO₂, samples show slightly less band gap energy than the un-doped SnO₂. The decrease in the band gap energy may be due to the accumulation of donor energy levels of TM ions in the actual band gap of SnO₂. Such band gap narrowing is also observed in case of Co doped ZnO thin films [16] and is attributed to the presence of Co at the cation site in the host matrix. In present case also, Fe and Ni are expected to present at Sn site of SnO₂ lattice, which is leading to the observed band-gap narrowing. It is clear from the above discussion that Fe and Ni ions have been incorporated in the SnO₂ lattice and affect the semiconducting properties of the material by tailoring the band gap energy.

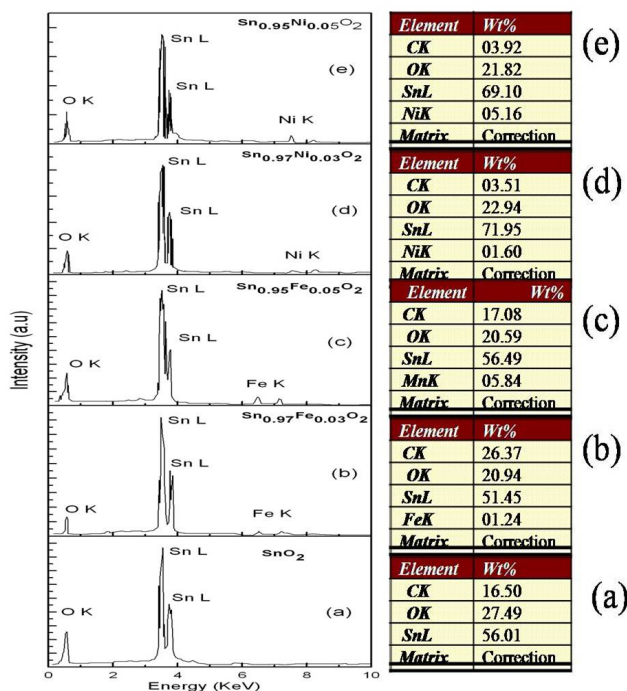


Figure 3. EDAX spectra of (a) SnO₂, (b) Sn_{0.97}Fe_{0.03}O₂ (c) Sn_{0.95}Fe_{0.05}O₂ (d) Sn_{0.97}Ni_{0.03}O₂ and (e) Sn_{0.95}Ni_{0.05}O₂, respectively.

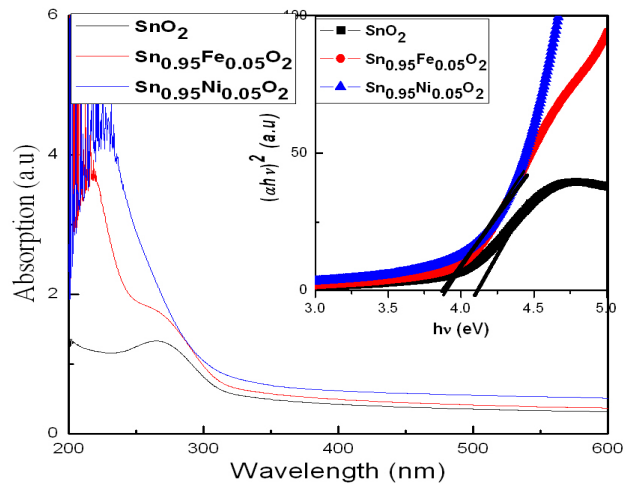


Figure 4. (Color online) UV-visible absorption spectra of SnO₂, Sn_{0.95}Fe_{0.05}O₂ and Sn_{0.95}Ni_{0.05}O₂ nanoparticles, respectively. The inset of the figure shows the Tauc's plot of the same samples.

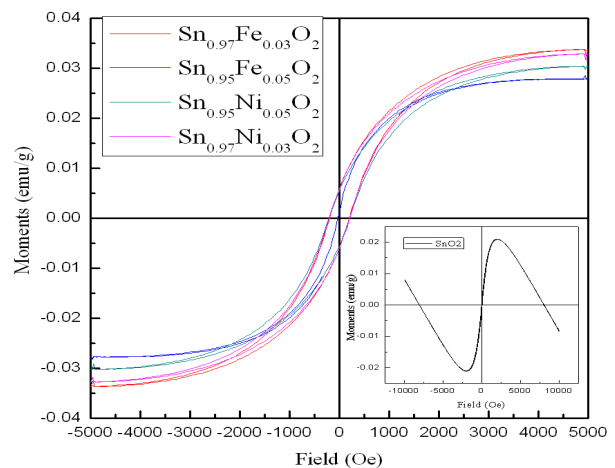


Figure 5. (Color online) Room temperature hysteresis curves of Sn_{0.97}Fe_{0.03}O₂, Sn_{0.95}Fe_{0.05}O₂, Sn_{0.97}Ni_{0.03}O₂ and Sn_{0.95}Ni_{0.05}O₂ nanoparticles. Inset of the figure shows hysteresis curve of un-doped SnO₂ nanoparticles.

To probe the magnetic properties of SnO₂, Sn_{0.97}Fe_{0.03}O₂, Sn_{0.95}Fe_{0.05}O₂, Sn_{0.97}Ni_{0.03}O₂ and Sn_{0.95}Ni_{0.05}O₂ nanoparticles, room temperature magnetization measurements were performed on the samples and are shown in Fig. 5. Inset of the Fig. 5 shows hysteresis loop for un-doped SnO₂ nanoparticles. It is clear from the inset of the Fig. 5 that un-doped SnO₂ show diamagnetic behaviour. This behaviour of un-doped SnO₂ arises due to the 4+ valance state of tin (Sn⁴⁺) which favours 4d¹⁰ electronic configuration of Sn in SnO₂ and, hence, there is no unpaired *d* electrons in the materials for any kind of ferromagnetic ordering. Ferromagnetic hysteresis loops were observed in Fe and Ni doped SnO₂ nanoparticles. The saturation magnetization and magnetic moments per Fe/Ni ions were found to decrease with increasing in the Fe and Ni concentration. The observed magnetic

moments are $0.029 \mu_B/\text{Fe}$, $0.014 \mu_B/\text{Fe}$, $0.028 \mu_B/\text{Ni}$, and $0.015 \mu_B/\text{Ni}$ for $\text{Sn}_{0.97}\text{Fe}_{0.03}\text{O}_2$, $\text{Sn}_{0.95}\text{Fe}_{0.05}\text{O}_2$, $\text{Sn}_{0.97}\text{Ni}_{0.03}\text{O}_2$ and $\text{Sn}_{0.95}\text{Ni}_{0.05}\text{O}_2$ nanoparticles, respectively. The higher magnetic moments, in case of $x = 0.03$ Fe and Ni doped samples, are may be due to the indirect exchange interaction among TM ions, mediated by O ions. As the TM ion concentration increases, the nearby two or more TM ions are expected to come closer sufficiently. If such TM atom pairs are present in the SnO_2 lattice, the well known super-exchange interaction is expected between them. The super-exchange interaction may lead to the anti-ferromagnetic type interaction among neighbouring TM-ions, leading to the observed decrease in magnetic moment with increasing TM concentration. The decrease in the magnetic moments of Fe and Ni ions, with increasing their doping concentrations, is consistent with our previously reported results of Co-doped SnO_2 nanoparticles [17], where we have observed a little reduction in the magnetic moments of Co ions, with increasing their doping concentrations. Therefore, the observed room temperature ferromagnetism in chemically synthesized Fe and Ni doped SnO_2 samples is intrinsic to the material and confirm the formation of SnO_2 based DMS systems.

4. Conclusions

Fe and Ni doped SnO_2 nanoparticles have been successfully synthesized using simple wet chemical method. Experimental findings indicate that Fe and Ni are incorporated into SnO_2 lattice without forming any TM cluster and/or oxide phases. TEM results indicate that very narrow distribution of spherically shaped nanoparticles (~ 3 nm) can be achieved by using co-precipitation method. The optical band gap energy found to decrease with increasing TM concentration, which may arise due to the formation of donor energy levels in the actual band gap of SnO_2 . Remarkably, room temperature ferromagnetism has been observed in Fe and Ni doped SnO_2 . It is reasonable to state that the, single phase, TM metal doped SnO_2 based DMS materials can be synthesized using the wet chemical method.

5. Acknowledgements

Authors (Aditya Sharma, Mayora Varshney and K. D. Verma) are thankful to Inter University Accelerator Center, New Delhi, India for providing financial assistance and experimental facilities under the UFUP projects (code-41304 and 46301).

6. References

- [1] G. A. Prinz, *Science* **282**, (1998) 1660.
- [2] S. A. Wolf, D. D. Awschalom, R. A. Buhrman, J. M. Daughton, S. V. Molnar, M. L. Roukes, A. Y. Chtcheljanova and D. M. Treger, *Science* **294**, (2001) 1488.
- [3] David D. Awschalom and Michael E. Flatté, *Nat. Phys.* **3**, 153 (2007).
- [4] J. K. Furdyna, *J. Appl. Phys.* **64**, R29 (1988).
- [5] Sanghoon Lee, J.-H. Chung, Xinyu Liu, Jacek K. Furdyna, and Brian J. Kirby, *Mat. Today* **12**, 14 (2009).
- [6] T. Dietl, H. Ohno, F. Matsukura, J. Cibert, and D. Ferrand, *Science* **287**, 1019 (2000).
- [7] D. C. Look and B. Claflin, *Phys. Stat. Sol. (b)* **241**, 624 (2004).
- [8] A. Punnoose, J. Hays, V. Gopal and V. Shutthanandan, *Appl. Phys. Lett* **85** (2004) 1559.
- [9] S. B. Ogale, R. J. Choudhary, J. P. Bhuvan, S. E. Lofland, S. R. Shinde, S. N. Kale, V. N. Kulkarni, J. Higgins, C. Lanci, J. R. Simpson, N. D. Browning, S. D. Sarma, H. D. Drew, R. L. Greene and T. Venkatesan, *Phys. Rev. Lett.* **91**, (2003) 077205.
- [10] Y. Xiao, S. Ge, Li Xi, Y. Zuo, X. Zhou, B. M. Zhang, Li Zhang, C. Li, X. Han, and Z. C. Wen, *Appl. Sur. Sci.* **254**, (2008) 7459.
- [11] J. M. D. Coey, A. P. Douvalis, C. B. Fitzgerald and M. Venkatesan, *Appl. Phys. Lett.* **84**, (2004) 1332.
- [12] K. Anandan, S. Gnanam, J. Gajendiran, and V. Rajendran, *J. Non-oxide Galsses*, **2** (2010) 83.
- [13] L. Jiang, G. Sun, Z. Zhou, S. Sun, Q. Wang, S. Yan, H. Li, J. Tian, J. Guo, B. Zhou, and Q. Xin, *J. Phys. Chem. B* **109** (2005), 8774.
- [14] H. Rath, P. Das, T. Som, P.V. Satyam, U. P. Singh, P. K. Kularia, D. Kanjilal, D. K. Avasthi, and N. C. Mishra, *J. Appl. Phys.* **105** (2009) 074311.
- [15] S. Das, S. Kar and S. Choudhary, *J. Appl. Phys.* **99**, (2006) 114303.
- [16] R. Kumar, F. Singh, B. Angadi, W. K. Choi, K. Jeong, J.-H. Song, M. W. Khan, J. P. Srivastava, A. Kumar and R. P. Tandon, *J. Appl. Phys.* **100**, (2006) 113708.
- [17] A. Sharma, A. P. Singh, P. Thakur, N.B. Brookes, S. Kumar, C. G. Lee, R. J. Choudhary, K. D. Verma and R. Kumar, *J. Appl. Phys.* **107** (2010) 093918.